Simulation of Spacecraft Attitude Measurement Data by Modeling Physical Characteristics of Dynamics and Sensors

Hungu Lee*, Jae-Cheol Yoon**, Yee-Jin Cheon**, Dongseok Shin*, Hyunjae Lee***, Young-Ran Lee*, Hyo-Choong Bang***, and Sang-Ryool Lee**

*Satrec Initiative Co. Ltd., 461-26 Jeonmin-dong, Yuseong-gu, Daejeon 305-811, Korea
(Tel : +82-42-365-7524; E-mail: budgie@satreci.com)
**Korea Aerospace Research Institute, 45 Eoeun-dong, Yuseong-gu, Daejeon 305-333, Korea
***Korea Advanced Institute of Science and Technology, Department of Aerospace Engineering, 373-1 Kusong-dong, Yuseong-gu, Daejeon 305-701, Korea

Abstract: As the remote sensing satellite technology grows, the acquisition of accurate attitude and position information of the satellite has become more and more important. Due to the data processing limitation of the on-board orbit propagator and attitude determination algorithm, it is required to develop much more accurate orbit and attitude determination, which are so called POD (precision orbit determination) and PAD (precision attitude determination) techniques. The sensor and attitude dynamics simulation takes a great part in developing a PAD algorithm for two reasons: 1. when a PAD algorithm is developed before the launch, realistic sensor data are not available, and 2. reference attitude data are necessary for the performance verification of a PAD algorithm. A realistic attitude dynamics and sensor (IRU and star tracker) outputs simulation considering their physical characteristics are presented in this paper, which is planned to be used for a PAD algorithm development, test and performance verification.

Keywords: Precision Attitude Determination, Satellite Attitude Dynamics, Sensor Output Simulation

1. INTRODUCTION

As the technology for developing earth observation spacecrafts grows faster ever before, the pointing and geo-location accuracy requirement becomes the major and critical concern in many applications. The accurate determination of the position, velocity and attitude of a spacecraft is essential in order to obtain accurately geo-located payload data (e.g. remotely sensed imagery) systematically and automatically. In general, the real-time on-board estimation of a spacecraft's orbit and attitude does not satisfy the accuracy requirement because a simplified model must be adopted due to the limited resources of the on-board processor and the lack of ancillary information. The restitution of accurate orbit and attitude information is, therefore, generally carried out at ground stations and it is called precision orbit determination (POD) and precision attitude determination (PAD), respectively.

In general, a POD algorithm can determine the position of a spacecraft with a meter-level accuracy, and hence a meter-level geo-location accuracy, by virtue of the relatively systematic movement of a spacecraft and the state-of-art technologies such as GPS, laser-ranging, and so on. However, the precise attitude determination with the accuracy of tens of arc-seconds (resulting in several tens of meters geo-location accuracy) is still challenging due to several factors; e.g. the high-frequency variation and perturbation of the attitude dynamics as well as the noise and stability characteristics of attitude sensors currently available. Therefore, the improvement of attitude determination accuracy is essential in order to achieve a comparable amount of ultimate geo-location uncertainty to the orbit determination.

The development of a PAD algorithm and software includes many technological aspects such as the precise modeling of attitude dynamics and sensor characteristics, the implementation of an attitude estimator such as a batch least square estimator or an extended Kalman filter, and the analytic and/or experimental determination of noise parameters. The verification and optimization of the developed PAD software shall be performed on the ground using simulated sensor data because it is impossible to obtain the true spacecraft's attitude during in-orbit operation. Thus the expectation of the ultimate success of PAD depends heavily on the degree of similarity between the simulated sensor data and real data to be obtained in near future.

The main focus of this paper is the generation of attitude sensor simulation data by using an as close model to the real situation as possible by implementing a fully physical modeling of the spacecraft attitude dynamics and measurement sensor noise characteristics. In this paper, it is assumed that the spacecraft has two star trackers pointed to different bore-sight direction for redundancy and one set of four gyros assembly, or an IRU (inertial reference unit), for spacecraft's rate information. Each star tracker is assumed to be able to generate both UVF (unit vector filter) and QUEST measurements. The output data from each gyro is assumed to be accumulated angle values rather than body rate values because they are assumed to be rate integrating gyros (RIGs). Precision orbit data samples are interpolated by using an 11^{th} order Lagrangian polynomial and used for the reference track of the satellite.

2. DEFINITION OF COORDINATES

The satellite has a main imaging payload of a push-broom type. The relative alignment angles between the bore-sight direction of the payload and the sensor mounting direction are measured on the ground using precise equipment such as theodolite. Usually, a mechanical body frame is thought as the reference coordinate system for those mounting directions when the satellite is integrated on the ground. However, when the satellite is operating on the space, the mechanical body frame becomes a fictitious coordinate system. Instead, the optical bench frame (OBF) of the satellite can be an alternative for the mechanical body frame because OBF can be measured accurately using the POD data and the ground control points (GCPs).

The satellite's attitude information is, therefore, defined as the OBF attitude with respect to an inertial celestial reference frame (CRF) such as J2000 coordinate. Let's denote the roll, pitch and yaw rotational angles as ϕ, θ, and ψ, respectively. Then the 321 Euler rotational matrix from CRF to OBF is expressed as:

$$\vec{\mathrm{x}}_{\mathrm{OBF}} = C_{CRF}^{OBF}(\phi,\theta,\psi)\vec{\mathrm{x}}_{\mathrm{CRF}}, \qquad C_{CRF}^{OBF}(\phi,\theta,\psi) = \begin{bmatrix} c\theta c\phi & c\theta s\phi & -s\theta \\ -c\psi s\phi + s\psi s\theta c\phi & c\psi c\phi + s\psi s\theta s\phi & s\psi c\theta \\ s\psi s\phi + c\psi s\theta c\phi & -s\psi c\phi + c\psi s\theta s\phi & c\psi c\theta \end{bmatrix} \tag{1}$$

Another expression of the rotational matrix of (1) using the attitude quaternion is expressed as [1]

$$C_{CRF}^{OBF}(\mathrm{q}) = \begin{bmatrix} q_1^2 - q_2^2 - q_3^2 + q_4^2 & 2(q_1q_2 + q_3q_4) & 2(q_1q_3 - q_2q_4) \\ 2(q_1q_2 - q_3q_4) & -q_1^2 + q_2^2 - q_3^2 + q_4^2 & 2(q_2q_3 + q_1q_4) \\ 2(q_1q_3 + q_2q_4) & 2(q_2q_3 - q_1q_4) & -q_1^2 - q_2^2 + q_3^2 + q_4^2 \end{bmatrix} \tag{2}$$

Two star trackers are mounted on the satellite with different bore-sight directions to compensate the poor angular accuracy around the bore-sight axes. The two star tracker coordinates are denoted as SCF1 and SCF2, respectively, and the rotational matrix from OBF (as the body frame) to SCF1 and SCF2 are specified as:

$$C_{OBF}^{SCF1} = \begin{bmatrix} -0.53908705 & 0.35008722 & -0.76604444 \\ -0.54463904 & -0.83867057 & 0 \\ -0.64245893 & 0.41721771 & 0.64278761 \end{bmatrix}$$
$$C_{OBF}^{SCF2} = \begin{bmatrix} 0.53908705 & 0.35008722 & -0.76604444 \\ -0.54463904 & 0.83867057 & 0 \\ 0.64245893 & 0.41721771 & 0.64278761 \end{bmatrix} \tag{3}$$

The rotation between OBF and SCF can also be expressed as quaternion as:

$$\begin{aligned} q_{OBF}^{SCF1} &= [-0.40521473 \quad 0.12003007 \quad 0.86898579 \quad 0.25740532]^T \\ q_{SCF1}^{OBF} &= [0.40521473 \quad -0.12003007 \quad -0.86898579 \quad 0.25740532]^T \\ q_{OBF}^{SCF2} &= [-0.12003007 \quad 0.40521473 \quad 0.25740532 \quad 0.86898579]^T \\ q_{SCF2}^{OBF} &= [0.12003007 \quad -0.40521473 \quad -0.25740532 \quad 0.86898579]^T \end{aligned} \tag{4}$$

The satellite has an inertial reference unit (IRU) measuring the satellite's body rate. The IRU has four sets of gyros, providing a full 3-axis inertial rate measurement with a redundancy. The relation between the IRU assembly coordinate system, or GCF (gyro coordinate system), and the four gyro measurement directions is specified as:

$$\vec{\omega}^{ABCD} = \begin{bmatrix} \omega_A \\ \omega_B \\ \omega_C \\ \omega_D \end{bmatrix} = C_{GCF}^{ABCD}\vec{\omega}^{GCF} = \begin{bmatrix} 0 & -\sqrt{\frac{2}{3}} & -\frac{1}{\sqrt{3}} \\ \frac{1}{\sqrt{2}} & \frac{1}{\sqrt{6}} & -\frac{1}{\sqrt{3}} \\ -\frac{1}{\sqrt{2}} & \frac{1}{\sqrt{6}} & -\frac{1}{\sqrt{3}} \\ 0 & 0 & 1 \end{bmatrix} \begin{bmatrix} \omega_x^{GCF} \\ \omega_y^{GCF} \\ \omega_z^{GCF} \end{bmatrix} \tag{5}$$

The mounting direction of the IRU with respect to OBF is specified as:

$$C_{OBF}^{GCF} = C_{GCF}^{OBF} = \begin{bmatrix} 1 & 0 & 0 \\ 0 & -1 & 0 \\ 0 & 0 & -1 \end{bmatrix} \tag{6}$$

3. ATTITUDE DYNAMICS

The satellite attitude is subject to the following Euler's dynamics model

$$\begin{aligned} \dot{\theta}_{body} &= \omega \\ \dot{\omega} &= I^{-1}(-\omega \times I\omega + t_c) \\ \dot{q} &= \tfrac{1}{2}\Omega(\omega)q \end{aligned} \tag{7}$$

where t_c is the control torque command for steering the payload to point an imaging target and

$$\Omega(\omega) \equiv \begin{bmatrix} 0 & \omega_z & -\omega_y & \omega_x \\ -\omega_z & 0 & \omega_x & \omega_y \\ \omega_y & -\omega_x & 0 & \omega_z \\ -\omega_x & -\omega_y & -\omega_z & 0 \end{bmatrix} \tag{8}$$

The integrated body angle, θ_{body}, is used to generate the IRU measurement data simulation because the considered gyro is assumed as an RIG (rate integrating gyro). For the accurate attitude data simulation, the attitude dynamics is integrated using 7-8th order Runge-Kutta method. The control torque command t_c is generated from the POD data to steer the satellite to point the nadir direction using a quaternion feedback control law [2].

4. IRU OUTPUT SIMULATION

The gyro angle outputs are corrupted by bias, angle random walk and angle white noise as well as the scale factor error and the IRU misalignment. The rate output of each gyro is calculated by the finite differentiation of the current and previous step angle values. All statistical values such as the sampling time stability, the scale factor variation and the gyro rate noise are modeled as white Gaussian random values. The IRU misalignment, which is caused mainly by thermal effect on the mechanical mounting interface of IRU, is modeled as a sinusoidal variation with the orbit period. The modeling of the scale factor errors takes the truncation effect of the analog-digital converter into account.

The gyro outputs are simulated as the following sequence:

1. The accumulated angle of GCF is obtained from the accumulated body angle by integrating (7) and converting to GCF as:
$$\theta_{GCF} = C_{OBF}^{GCF}\theta_{body}$$
2. Apply IRU misalignment as:
$$\theta'_{GCF} = (I - [\delta_{GCF}\times])\theta_{GCF}$$
where the small angle rotational matrix is approximated by using a matrix representation of the vector cross product.
3. Convert GCF angles into gyro angles:
$$\theta_{ABCD} = C_{GCF}^{ABCD}\theta'_{GCF}$$
4. Convert the gyro angle into 16-bit counter (0~65535) by truncating with an LSB of 0.05 arc-sec.
5. Apply scale factor error to the truncated angle outputs.
6. Propagate angle drift by integrating the angle bias stability and angle random walk as:

$$b_{k+1} = b_k + \Delta t_k N(0, \sigma_b) + \sqrt{\Delta t_k} N(0, \sigma_{rw})$$

where Δt_k is the integration step at time t_k, σ_b is the standard deviation of the bias stability and σ_{rw} is the standard deviation of the angle random walk. A simple Euler's integration method is used for the angle drift integration and the random time offset error of 20 ms from the nominal output time is also considered.

7. Add angle drift and angle white noise to the truncated gyro angle outputs.
8. Simulate gyro rate outputs using finite difference method as:

$$\omega_{ABCD} = \frac{\theta_{ABCD} - \theta_{ABCD\,prev}}{\Delta t} \tag{9}$$

Note that the time step used for the rate output generation is the nominal value because the output time offset information is not available.

The nominal noise characteristics for the IRU are presented in Table 1.

Table 1 The noise characteristics of the IRU.

Characteristics	**Value**
Angle Random Walk (deg/hr$^{1/2}$)	0.0003
Angle White Noise (arc-sec/Hz$^{1/2}$)	0.014
Bias Stability (deg/hr, 1σ)	0.0006
Scale Factor Error (ppm, 1σ)	30
Readout Frequency (Hz)	20

5. STAR TRACKER OUTPUT SIMULATION

The measurement data of the star trackers are simulated from the attitude quaternion generated by integrating Eq. (7). For the star tracker output noise, three different noise terms are considered: bias, low frequency noise and noise equivalent angle (NEA):

- Bias errors: alignment uncertainties, biases, and all errors which frequency is lower than the orbital period. These errors are identical for each measured star.
- Low frequency noise: all errors which frequency is higher than or equal to the orbital period and lower than 20 seconds.
- NEA: all errors which frequency is higher than 20 seconds. NEA captures only effects due to photon noise, stray light noise, dark current noise, and readout noise.

Bias is assumed as a fixed value during the sensor data generation and the low frequency noise as a first-order Markov process having a time constant longer than 20 seconds. NEA is generated by applying a Gaussian random process at every measurement time. The random time offset error of 20 ms is also applied to both star tracker outputs. Note that the time offsets of the two star trackers are set differently.

Two types of star tracker measurements are provided:

- 3 axes quaternion measurement by the star tracker QEST algorithm, denoted as QUEST output
- 2 axes normalized star measurement (center position at the CCD frame), denoted as UVF output

The concrete descriptions of the two types of the star tracker output simulations are presented in the following subsections.

5.1 QUEST Output

QUEST measurement is simulated from the attitude quaternion of OBF by integrating the attitude dynamics of Eq. (7). The concrete simulation sequence is as follows:

1. Convert the integrated body quaternion to the nominal SCF direction as:

$$q_{SCF_0} = q_{OBF}^{SCF_0} \otimes q$$

where, $\otimes$ is the quaternion product.

2. Apply misalignment error as:

$$q_{SCF} = q_{SCF_0}^{SCF} \otimes q_{SCF_0}$$

where,

$$q_{SCF_0}^{SCF} \approx \begin{bmatrix} \frac{1}{2}\delta_{SCF} \\ 1 \end{bmatrix}$$

3. Calculate measurement noise vector as:

$$\vec{v}_{SCF} = \vec{v}_{bias}^{QUEST} + \vec{v}_{LFN}^{QUEST} + \vec{v}_{NEA}^{QUEST}$$

where the low frequency noise is obtained by integrating the following first-order Markov process as:

$$\dot{\vec{v}}_{LFN}^{QUEST} = -(1/\tau_{LFN}^{QUEST})\vec{v}_{LFN}^{QUEST} + \vec{v}_{LFN}^{QUEST} \tag{10}$$
$$\vec{v}_{LFN}^{QUEST} \sim N(0, \sigma_{LFN})$$

A simple Euler's integration method is used for the integration of Eq. (10).

4. Convert the measurement noise vector into the quaternion q_v.
5. Apply QUEST measurement noise as:

$$q_{SCF}^{QUEST} = q_v \otimes q_{SCF}$$

The QUEST noise characteristics of the star tracker output simulation are presented in Table 2.

Table 2 The QUEST noise characteristics of the star tracker

Characteristics	**Value**
Bias	
Vertical to the bore-sight direction	15 arc-sec
Around the bore-sight direction	13 arc-sec
Low Frequency Errors (3σ)	
Vertical to the bore-sight direction	9 arc-sec
Around the bore-sight direction	33 arc-sec
NEA (3σ)	
Vertical to the bore-sight direction	12.5 arc-sec
Around the bore-sight direction	86 arc-sec

For the simulation of the low frequency noise, the driving noise characteristics σ_{LEN} shall be determined from the resulting noise characteristics. As the integration of the low frequency noise is done by Euler's method, the driving noise characteristics are determined from the actual low frequency noise characteristics as

$$\sigma_{LFN} = \sigma_{LFN}^{QUEST} \sqrt{\frac{2}{\tau_{LFN}^{QUEST} \Delta T} - \left(\frac{1}{\tau_{LFN}^{QUEST}} \right)^2} \qquad (11)$$

5.2 UVF (Unit Vector Filter) Output

For the UVF measurement, 10 brightest stars within the star tracker's field of view are generated from the user defined star catalog. The NEA standard deviation applied for the UVF measurements simulation is varying according to the star magnitude and interpolated from the nominal values presented in Table 3.

Table 3 The UVF noise characteristics of the star tracker

Characteristics	Value
Bias	
Vertical to the bore-sight direction	15 arc-sec
Around the bore-sight direction	13 arc-sec
Low Frequency Errors (3σ)	
Vertical to the bore-sight direction	9 arc-sec
Around the bore-sight direction	33 arc-sec
NEA (3σ)	
Mv = 6	117 arc-sec
Mv = 5.5	61 arc-sec
Mv = 5	40 arc-sec
Mv = 4.5	26 arc-sec
Mv = 4	19 arc-sec
Mv = 3.5	16 arc-sec
Mv = 2.5	12 arc-sec
Mv = 1	9 arc-sec
Mv =0 .1	9 arc-sec

The detailed simulation procedure for the UVF output generation is as follows:

1. Convert body quaternion into the nominal star tracker frame.
2. Select 10 brightest stars within the field-of-view (FOV). FOV is set as circular 25 deg.
3. For each selected star, calculate the star unit vector at the star catalog frame (J2000 frame) as:
$$u_x^{CRF} = \cos\theta\cos\phi$$
$$u_y^{CRF} = \cos\theta\sin\phi$$
$$u_z^{CRF} = \sin\theta$$
4. Transform the unit vector to the nominal SCF direction as:
$$\mathbf{u}^{SCF_0} = C_{CRF}^{SCF_0}\mathbf{u}^{CRF}$$
5. Apply misalignment error as:
$$\mathbf{u}^{SCF} = (I - [\delta_{SCF}\times])\mathbf{u}^{SCF_0}$$
6. Calculate UVF measurement noise as:
$$\vec{v}_{SCF} = \vec{v}_{bias}^{UVF} + \vec{v}_{LFN}^{UVF} + \vec{v}_{NEA}^{UVF}$$
where the low frequency noise is obtained by integrating the following first-order Markov process as:
$$\dot{\vec{v}}_{LFN}^{UVF} = -(1/\tau_{LFN}^{UVF})\vec{v}_{LFN}^{UVF} + \vec{v}_{LFN}^{UVF}$$
$$\vec{v}_{LFN}^{UVF} \sim N(0, \sigma_{LFN}) \qquad (12)$$
A simple Euler's integration method is used for the integration of Eq. (12). The driving noise characteristics is set as:
$$\sigma_{LFN} = \sigma_{LFN}^{UVF} \sqrt{\frac{2}{\tau_{LFN}^{UVF} \Delta T} - \left(\frac{1}{\tau_{LFN}^{UVF}} \right)^2} \qquad (13)$$
7. Add UVF measurement noise into the UVF output.

When any of the 10 stars goes outside the star tracker's FOV, the initialization of UVF output for selecting 10 brightest stars is performed again.

6. SIMULATION SOFTWARE DEVELOPMENT

The simulation software is developed as a configurable form in which all parameters such as noise standard deviations, nominal sensor mounting attitudes, measurement sampling frequency and so on can be modified and applied through graphical user interface. The value and variation of each resultant parameter can also be analyzed statistically and graphically. The software's flow diagram is presented in Fig. 1.

Fig. 1 Simulation Flow Diagram.

7. SAMPLE SENSOR DATA GENERATION

A sample attitude and sensor data is simulated and generated. Each graph displays the RMS value of the sensor noise and thus the simulated sensor noise characteristics are verified.

Fig. 2 shows the POD data in ECEF (Earth centered Earth fixed) frame used for the attitude command generation. The assumed orbit is an LEO sun-synchronous. The data used for the sample generation is for 15 minutes.

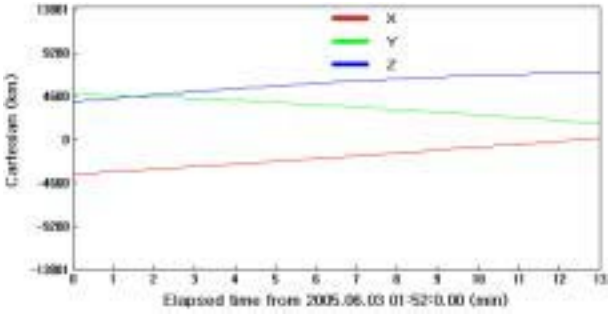

Fig. 2 Sample POD data (ECEF frame).

Fig. 3 shows the spacecraft's attitude (3-axis Euler angles) and Fig. 4 shows the Earth pointing roll, pitch and yaw attitude in LVLH (local vertical local horizontal) frame. The error in pitch attitude is due to the delay in the quaternion feedback control law.

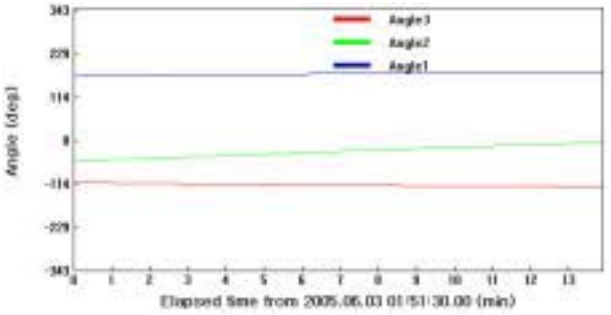

Fig. 3 Spacecraft attitude (Euler angles).

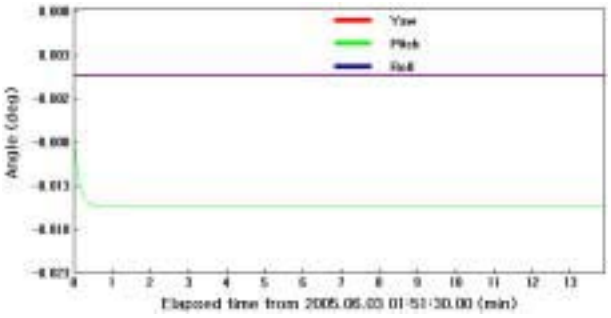

Fig. 4 Roll, pitch and yaw attitude in LVLH frame.

Fig. 5 and Fig. 6 shows the gyro angle and rate outputs, respectively. The peak in gyro rate output is due to the false sensor data.

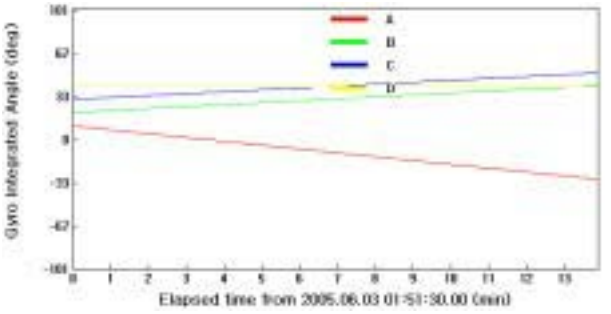

Fig. 5 Gyro angle output.

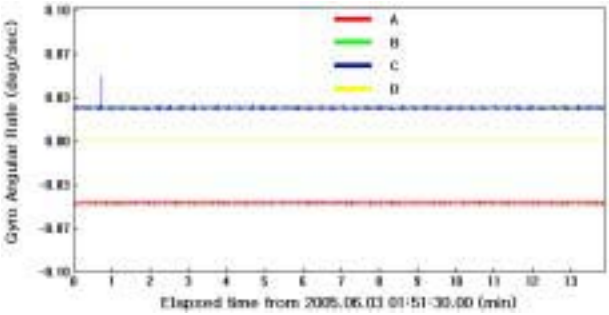

Fig. 6 Gyro rate output.

The QEST outputs of the two star trackers are shown in Fig. 7 and Fig. 8, respectively, which do not clearly show the noise characteristics.

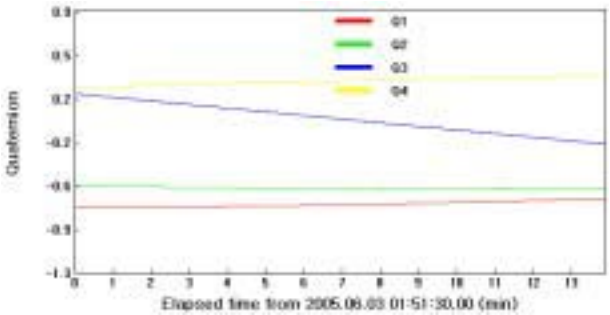

Fig. 7 QEST output of star tracker 1

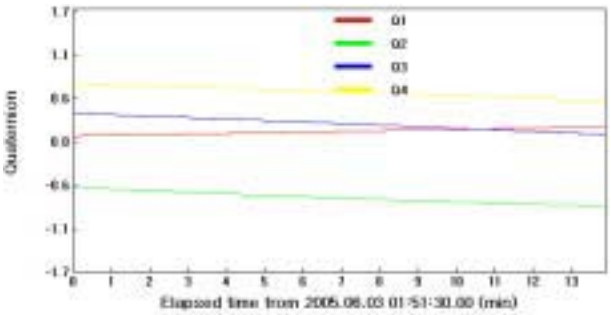

Fig. 8 QEST output of star tracker 2

Fig. 9 and Fig. 10 shows the low frequency noise and NEA of the star tracker. The calculated RMS values verify that the generated noise simulates the sensor characteristics correctly.

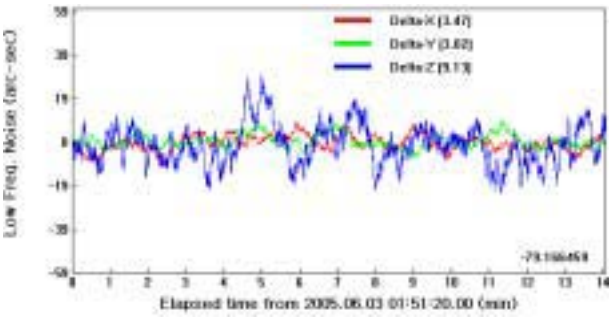

Fig. 9 Low frequency noise of the star tracker 1 QUEST output.

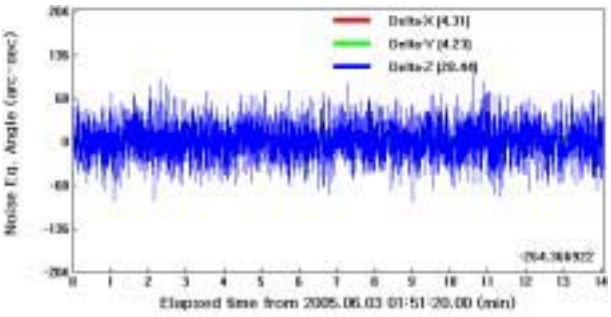

Fig. 10 NEA of the star tracker 1 QEST output.

The same noises for UVF are displayed in Fig. 11 and Fig. 12. The nominal star magnitude for NEA noise in Fig. 12 was set as 2.5, though the NEA characteristics are generated by interpolation according to the star magnitude.

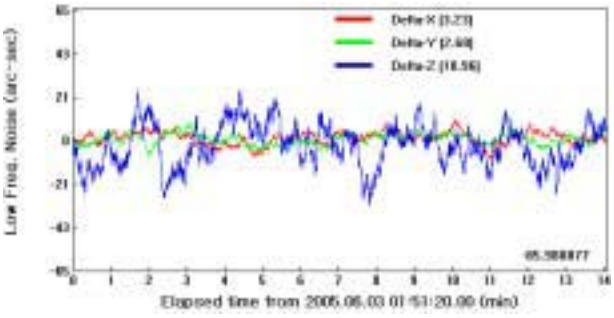

Fig. 11 Low frequency noise of the star tracker 1 UVF output.

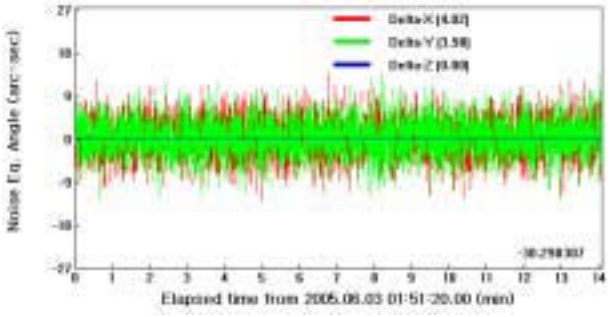

Fig. 12 NEA of the star tracker 1 UVF output (Mv =2 .5).

The star tracker misalignment profiles are also generated as Fig. 13 and Fig. 14. The profiles are generated as the sinusoidal patterns having one orbit period by assuming that the main source of the misalignment variation is the illumination condition. The misalignment profiles will be used as the reference data for the misalignment estimation using a PAD algorithm.

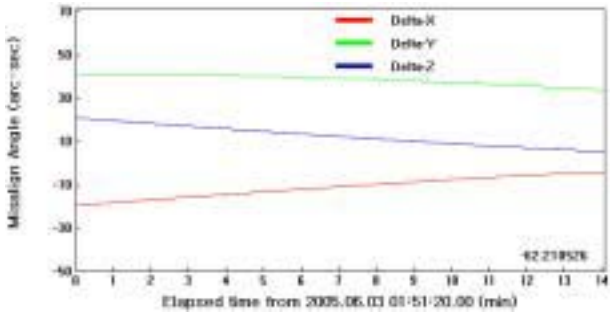

Fig. 13 Misalignment profile of the star tracker 1.

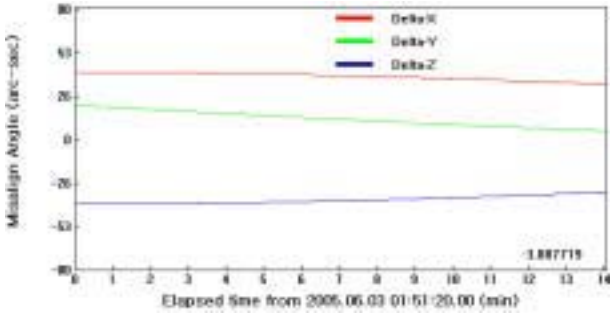

Fig. 14 Misalignment profile of the star tracker 2.

8. CONCLUSIONS

A realistic attitude sensor output simulation technique is proposed by considering the physical characteristics of the attitude dynamics and sensors. The simulated sensor and reference attitude data can be used for test and performance verification of precision attitude determination algorithm. The presented method is expected to play an important role for testing and validating when developing a PAD algorithm.

ACKNOWLEDGMENTS

The works in this paper was supported by KOMPSAT system integration department of KARI (Korea Aerospace Research Institute), Daejeon, Korea.

REFERENCES

[1] J. R. Wertz, *Spacecraft Attitude Determination and Control*, Kluwer Academic Publishers Group, Dordrecht, Holland, 1978.

[2] B. Wie, H. Weiss, and A. Arapostathis, "Quaternion Feedback Regulator for Spacecraft Eigenaxis Rotations," *J. Guidance, Control and Dynamics*, Vol. 12, No. 3, pp. 375-380, May-June 1989.